Nonlinear Behaviors of a Small Wind Turbine Induced by Aerodynamics and Electromagnetic Field

Yung-Chia Hsiao[1], Lih-Shyng Shyu[2]

[1] School of Materials Science and Engineering, Baise University, China
[2] Department of Material and Energy Engineering, MingDao University, Taiwan
1879320336@qq.com, lsshyu@mdu.edu.tw

Abstract

Modern small wind turbines output maximum electricity with the use of optimal controllers such as maximum power point tracking. A windmill would rotate at a speed around an optimal value for a specific wind speed under the control algorithms. Some of the average rotational speeds far beyond the optimal value were remarked at light wind in some field tests, and the variety of the speed dissolves as moderate or fresh breeze blowing repeatedly. The phenomenon could bring about passive optimal control failure. Furthermore, some investigations observed a hysteresis consisted of a couple of saddle-node bifurcations which are induced by nonlinear aerodynamics of the small windmill at different electricity output. This paper analyzed the behaviors of a small wind turbine through considering the coupling of the aerodynamics of the windmill and the electromagnetic field of a permanent magnet synchronize generator via a nonlinear mathematic model. More than two saddle-node bifurcations exist in the wind turbine system. Two sets of the saddle-node bifurcations separate the equilibrium points of the system into three leading branches. Moreover, two Hopf bifurcations were observed as well. The bifurcations induce the whirling speeds of the turbine spread over the lower leading branch of the equilibrium points. Meanwhile, a jump phenomenon from the saddle-node bifurcation clears up the variation at blowing fresh breeze. The bifurcation diagram demonstrates the reason that the variant whirling speeds were detected only at light breeze. The observed phenomena would inspire different optimum control design of small wind turbines.

Keywords: Small windmill, Aerodynamics, Permanent magnet synchronize generator, Saddle-node bifurcation, Hopf bifurcation

1 Introduction

Nowadays, many disasters induced by the change of climate forces countries to face up to the global warming which results from a lot of pollution of methane, nitric oxide and carbon dioxide, and leads people to seriously look at renewable energy which is abundantly available and clean in nature; for instance, biomass, wind energy, and solar power to which the wind power is a vital source. A rotor system captures wind energy and converts it into rotational kinetic energy which drive an electrical generator. The electricity output is conducted to storage devices like batteries, or to the power grid through grid-tide inverters. Large wind turbines are the most widespread type due to their lots of power over 500 kW, low cost per kWh and high efficiency. Furthermore, noise from the rotation of the windmill and high cut-in speed of the turbines bring about the demand of the desired wind farms beyond urban areas and with steady strong wind.

Small wind turbines whose power is under 100kW, on the other hand, are more appropriate to the urban areas compared with the large turbines because of their low cut-in speed. Lately, they more and more frequently appear around schools, villages, and exurban houses where are close to the load they supply. People do not like to live in areas that have high wind. Gentle wind oftentimes blows the small rotor; Consequently, the motion of the wind rotor in light breeze blowing is noteworthy to small wind turbines.

For high efficient small wind turbines, an optimal controller such as a maximum power point tracking (MPPT) is applied to modulate the rotational speed of the windmill around an optimal value for a specific wind speed under the control algorithms. Under the optimal control, however, the gyration of a small windmill blown by little wind is disorderly as reported by some field tests [1-3]. Starting windmill when the blow begins requires powerful wind than preserving the rotor whirling as wind is dieing, i.e., the mean whirling speeds of the rotor would be different at a specific low wind speed, as declared in the investigations of a horizontal axis wind turbine by Wright and Wood [1-2]. In addition, Shyu et al. recorded an alike phenomenon for a vertical axis turbine too [3]. By contrast, the alteration of the whirling speeds vanishes in a constant blow of

*Corresponding Author: Yung-Chia Hsiao; E-mail: 1879320336@qq.com
DOI: 10.3966/160792642020012101004

moderate or fresh breeze. Wright and Wood became conscious that a high angle of attack of the blades induces difficult starting. Instead of studing the cause of the variety as light breeze blows, they were devoted to design an optimal airfoil to increase the lift coefficient of the blades. Besides, Samsonov et al. studied a aerodynamic modelling of a small wind turbine and indicated that two saddle-node bifurcation points induce a hysteresis in variant electric output for the small wind rotor [4]. The bifurcation points join stable and unstable equilibrium points together, and meanwhile two sets of the stable points place on both sides of the unstable points. The stable sets coexist and result in the previous varied rotation of the wind rotor. What's more, once the rotor begins to whirl from rest, the coexistence induces the consistently slow rotation of the windmill although blowing gentle breeze instead of light wind.

Samsonov et al. studied the small wind turbine in which a windmill coupled a linear DC generator. Modern practice, however, favours permanent magnet synchronize generators (PMSGs) instead of DC generators for small wind turbines. Permanent magnet synchronize machines are well known for their strong nonlinearity and coupling between mechanical and electrical subsystems. The nonlinearity of the PMSG would be important to the dynamics of the wind turbine. Many investigations observed bifurcations and chaos for the synchronize machines [5-12]. Li et al. first derived the modelling of a permanent magnet synchronize motor (PMSM) adapted for performing the bifurcation and chaos analysis [5]. After an affine transformation, the dimensionless model is similar to the famous Lorenz system as setting the quadrature- and direct -axis stator voltages, and the external load of the motor to zeros or deterministic values. The other studies designed some controllers to suppress the nonlinear behaviours of the PMSM [6-9]. In contrast, the phase of the moment produced by the PMSG is opposite to the torque by the PMSM. The inverse phase of the moments induces different dynamics of the PMSG to the PMSM. Although some investigations studied the nonlinear dynamics of the PMSGs for wind turbines [10-12], they studied only the nonlinear electromagnetic field of the generators, but not including the nonlinear aerodynamics of the windmill.

This study looked into why the fluctuant whirling speeds of the wind rotor appear or vanish in different wind speeds by observing a bifurcation diagram consist of Hopf and saddle-node bifurcations. Based on a nonlinear modelling of a small windmill coupled a PMSG, the equilibria of the wind turbine were detected, and their stability, in the meantime, was discerned by the Jacobin matrixes themselves. Consequently, the saddle-node and Hopf bifurcations were observed at particular wind speeds. More than two saddle-node bifurcations were detected in this system. Two Hopf bifurcations were observed as well. A bifurcation diagram constructed by the bifurcations are obtained with different wind speeds through the detection of the equilibria and bifurcations [13]. The results of the analysis disclose why the wide-ranging whirling speeds were looked only at light wind.

The remainder of this paper is organized in the following. Section 2 recounts the nonlinear modelling of a small windmill coupled a PMSG. Section 3 expresses the approaches of analyzing the dynamics of the wind turbine system. Section 4 ascertains the appearance and disappearance of the varied rotational speeds of the windmill. Finally, conclusion is shown in Section 5.

2 Modelling of a Small Windmill Coupled a PMSG

Differential equations for a small horizontal axis windmill coupled a PMSG derived from the d-q model [10, 14] is showed as follows,

$$\begin{cases} J\dfrac{d\omega}{dt} = M(\alpha,\omega) - [n_p \cdot \lambda_0 \cdot i_q + n_p(L_d - L_q) i_d \cdot i_q] - B \cdot \omega & \textbf{(1a)} \\ L_q \dfrac{di_q}{dt} = -r \cdot i_q - n_p \cdot \omega \cdot L_d \cdot i_d + n_p \cdot \omega \cdot \lambda_0 - u_q & \textbf{(1b)} \\ L_d \dfrac{di_d}{dt} = -r \cdot i_d + n_p \cdot \omega \cdot L_q \cdot i_q - u_d & \textbf{(1c)} \end{cases}$$

where J, ω, and B are respectively the rotational inertia, the whirling speed, and the friction coefficient of the windmill. n_p and λ_0 is the number of pole pairs of the rotor and rotor permanent magnet flux. i_d and i_q are generator currents over d- and q-axes. L_d and L_q are stator inductances over d- and q- axes. r is the resistance of the windings of the stator. u_d and u_q are generator voltages over d- and q- axes. The moment coming from the rotor denoted as the symbol M is estimated in the following,

$$M = \frac{1}{2}\rho \cdot A \cdot b \cdot V_r^2 [C_l(\alpha)\cos(\varphi - \alpha) - C_d(\alpha)\sin(\varphi - \alpha)] \quad \textbf{(2)}$$

where A represents the cross-section area of the rotor, ρ is air density, b is the distance betwixt the pressure center of blades and the hub axis, and φ designates the pitch angle of the blades. Figure 1 depicts C_d and C_l that are the drag and lift coefficients of the blades of using NACA0018 aerofoil, respectively [15]. The relative wind speed V_r to the rotor and the attack angle α are displayed as follows,

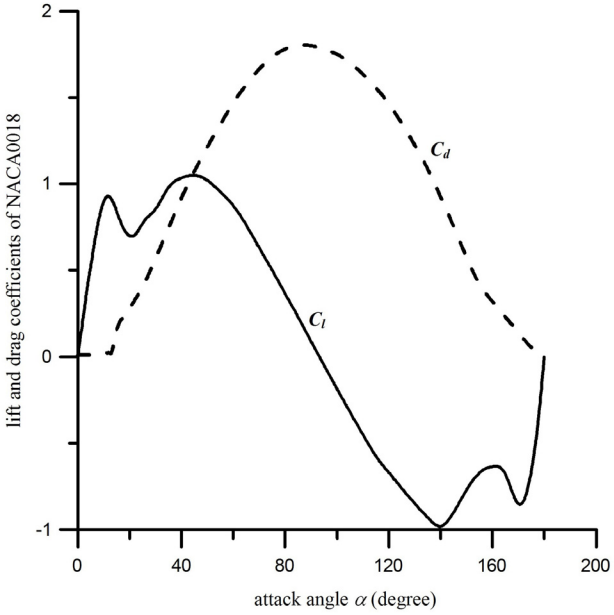

Figure 1. Coefficients C_l amd C_d of the NACA0018 aerofoil. The solid line denotes the lift coefficient C_l. The dash line displays the drag coefficient C_d. The curves of the coefficients are interpolated using cubic spline based on the experiment data by R. E. Sheldahl and P. C. Klimas [15]

$$V_r = \sqrt{(b\omega)^2 + V_w^2} \tag{3}$$

$$\alpha = \varphi - \tan^{-1}(\frac{b\omega}{V_w}) \tag{4}$$

where V_w indicates wind speed. Table 1 represents the parameters used in Eqs. (1a), (1b), (1c), and (2).

Table 1. Parameters used in the small wind power system

parameters	values
ρ	1.293 (kg/m^3)
A	19.63 (m^2)
b	1.5 (m)
J	0.5 (kg · m^2)
B	0.1 (N-m·sec/rad)
φ	$\frac{\pi}{2} - 0.1$ (rad)
np	21
λ0	0.4382 (Wb)
Ld, Lq	0.04156 (H)
r	0.9 (Ω)
ud	100 (V)
uq	100 (V)

3 Analysis Methods for the Wind Power System

An equilibrium point (ω^*, i_q^*, i_d^*) of the wind power system is found out through finding zeros of the equations given below,

$$\begin{cases} M(\alpha,\omega) - [n_p \cdot \lambda_0 \cdot i_q + n_p(L_d - L_q) i_d \cdot i_q] - B \cdot \omega = 0 & \textbf{(5a)} \\ -r \cdot i_q - n_p \cdot \omega \cdot L_d \cdot i_d + n_p \cdot \omega \cdot \lambda_0 - u_q = 0 & \textbf{(5b)} \\ -r \cdot i_d + n_p \cdot \omega \cdot L_q \cdot i_q - u_d = 0 & \textbf{(5c)} \end{cases}$$

Substituting Eqs. (5b) and (5c) into Eq (5a), the equations are rewritten as follows,

$$\begin{cases} M(\alpha,\omega) \cdot (r + \frac{n_p^2 \cdot \omega^2 \cdot L_d \cdot L_q}{r}) - n_p \cdot \lambda_0 \cdot i_q \cdot (\frac{n_p \cdot \omega \cdot L_d \cdot u_d}{r} + n_p \cdot \omega \cdot \lambda_0 - u_q) - \\ n_p(L_d - L_q) \cdot (\frac{n_p \cdot \omega \cdot L_q \cdot i_q - u_d}{r}) \cdot (\frac{n_p \cdot \omega \cdot L_d \cdot u_d}{r} + n_p \cdot \omega \cdot \lambda_0 - u_q) - B \cdot \omega \cdot (r + \frac{n_p^2 \cdot \omega^2 \cdot L_d \cdot L_q}{r}) = 0 & \textbf{(6a)} \\ i_q = \dfrac{\frac{n_p \cdot \omega \cdot L_d \cdot u_d}{r} + n_p \cdot \omega \cdot \lambda_0 - u_q}{r + \frac{n_p^2 \cdot \omega^2 \cdot L_d \cdot L_q}{r}} & \textbf{(6b)} \\ i_d = \dfrac{n_p \cdot \omega \cdot L_q \cdot i_q - u_d}{r} & \textbf{(6c)} \end{cases}$$

The values of (ω^*, i_q^*, i_d^*) are calculated by the three successive Eqs. (6a), (6b) and (6c). To disturb the point lightly, this paper replaced (ω, i_q, i_d) as ($\omega^*+\delta\omega$, $i_q^*+\delta i_q$, $i_d^*+\delta i_d$) in Eqs. (1a), (1b) and (1c). $\tilde{\boldsymbol{x}} = (\delta\omega, \delta i_q, \delta i_d)$ symbolizes the small disturbance. The perturbed system is depicted as follows after reserving the linear terms only,

$$\dot{\tilde{\boldsymbol{x}}} = M_J \cdot \tilde{\boldsymbol{x}}, \tag{7}$$

where M_J is referred a Jacobin matrix respective to the point (ω^*, i_q^*, i_d^*) shown in the following.

$$M_J = \left[\begin{array}{ccc} \frac{1}{J}\left(\frac{\partial M(\alpha,\omega)}{\partial\omega} - B\right) & -\frac{n_p\cdot\lambda_0 + n_p(L_d - L_q)i_d}{J} & 0 \\ \frac{-n_p\cdot L_d\cdot i_d + n_p\cdot\lambda_0}{L_q} & \frac{-r}{L_q} & \frac{-n_p\cdot\omega\cdot L_d}{L_q} \\ \frac{n_p\cdot L_q\cdot i_q}{L_d} & \frac{n_p\cdot\omega\cdot L_q}{L_d} & \frac{-r}{L_d} \end{array}\right]\Bigg|_{\substack{\omega=\omega^* \\ i_q=i_q^* \\ i_d=i_d^*}}, \tag{8}$$

The characteristic equation of $\boldsymbol{M}_J$ is written in the following,

$$\left|\lambda\cdot I - M_J\right| = 0 \tag{9}$$

where λ represents an eigenvalue of the point itself. An equilibrium point changes its stablility if the real part of any eigenvalue of its Jacobin matrix reverses the sign itself based on the bifurcation theory [16]. Two ways where the hyperbolicity condition can be flouted. Either Hopf bifurcation occurs as a pair of complex eigenvalues arrives the imaginary axis of the complex plane; Or transcritical bifurcation, saddle-node bifurcation or pitchfork bifurcation occurs when a simple real eigenvalue is located zero. Equilibrium points and bifurcation points could be detected simultaneously after plugging the foresaid critical eigenvalue into Eq. (9) [13].

4 Nonlinear Behaviors of the Small Windmill Caused by Electromagnetic Field and Aerodynamics

This paper studied the variation of the equilibrium points of the windmill through looking for the solutions of Eqs. (6a), (6b), and (6c) by the Newton's method under variant wind speeds in order to find out the origination which makes the wide-ranging whirling speeds of the wind turbine appear or vanish. The bifurcations were found from the stability analysis using Eq. (9) and the previous equations illustrated in Sec. 3. A bifurcation diagram described in Figure 2(a), which portrays eight saddle-node bifurcation points $P_{sn,a}$, $P_{sn,b}$, $P_{sn,c}$, $P_{sn,d}$, $P_{sn,e}$, $P_{sn,f}$, $P_{sn,g}$ and $P_{sn,h}$ on the ends of the branches composed of the equilibria, displays how the bifurcation points result in the appearance and disappearance of the disorderly whirling of the wind rotor. Figure 2(b) magnifies a part of Figure 2(a) surrounding the saddle-node bifurcations to demonstrate the dynamics of the windmill in little wind. At low wind speeds, some different equilibrium points exist together betwixt the bifurcation points $P_{sn,a}$ and $P_{sn,h}$. Three leading branches identified as ω_{s1}^*, ω_{u1}^* and ω_{s2}^* are on place in falling order of number betwixt the points $P_{sn,a}$ and $P_{sn,b}$. The stablility of the equilibrium points in each of the breanches is equal except the breanch ω_{s2}^*. Two supercritical Hopf bifurcation points denoted as $P_{H,a}$ and $P_{H,b}$ placed on the branch ω_{s2}^*, and divide the branch into three segments $\omega_{s2,a}^*$, $\omega_{s2,b}^*$, and $\omega_{s2,c}^*$. The equilibrium points $\omega_{s2,b}^*$ is situated between the points $\omega_{s2,a}^*$, and $\omega_{s2,c}^*$. Three of the leading branches, ω_{s1}^*, $\omega_{s2,a}^*$, and $\omega_{s2,c}^*$, are stable and the others, ω_{u1}^* and $\omega_{s2,b}^*$, are unstable. In the right side of the bifurcation point $P_{sn,b}$, other branches composed of the other stable or unstable equilibrium points, labeled as ω_{s3}^*, ω_{s4}^*, ω_{s5}^*, ω_{u2}^*, ω_{u3}^*, and ω_{u4}^*, are alternately arranged like a contour of an open palm. Furthermore, individual stable equilibrium point persists in the others eventually. Consequently, a broad boundary consisting of the unstable points ω_{u1}^* and ω_{u2}^* is stationed betwixt the attraction regions of the branches ω_{s1}^*, $\omega_{s2,a}^*$, $\omega_{s2,b}^*$, and $\omega_{s2,c}^*$.

When the wind starts blowing, the leading branches $\omega_{s2,a}^*$, $\omega_{s2,b}^*$, and $\omega_{s2,c}^*$ dominate the rotary motion of wind rotor when the blades begin to rotate or slowly whirl. The wide boundary induces gradually accelerating rotation of the windmill even though gentle breeze blows instead. Therefore the output of the small wind turbine would be limited. Nevertheless, customers wish to watch their wind turbines whirling fast once blowing gentle breeze rather than caring about the actual electricity output. The broad line causes damage to manage small wind rotors optimally. The condition is more serious about passive algorithms

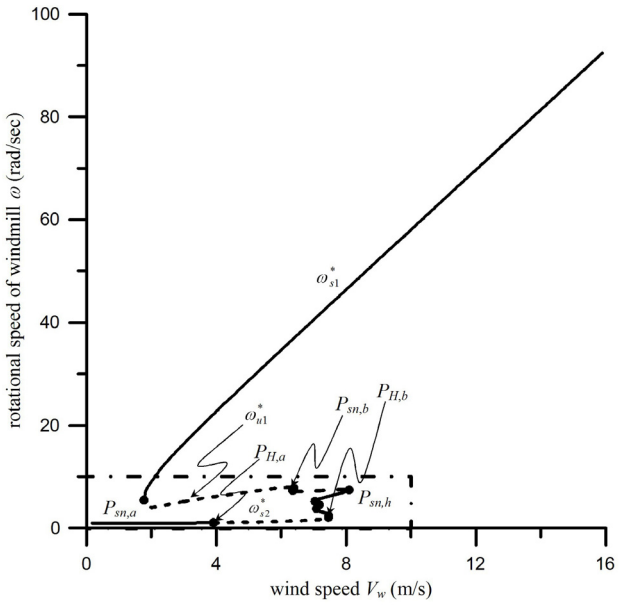

(a)

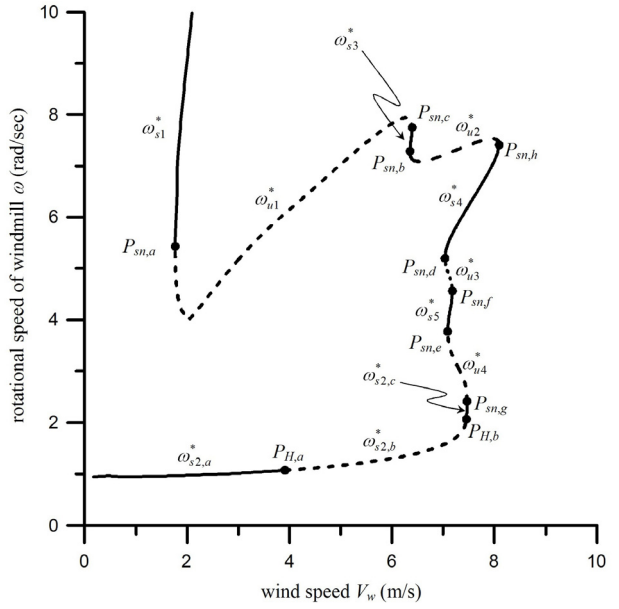

(b)

Figure 2. (a) Bifurcation diagram at variant wind speed for the small windmill. (b) a blow-up of Figure 2(a). The solid lines represent stable equilibria ω^*_{s1}, $\omega^*_{s2,a}$, $\omega^*_{s2,c}$, ω^*_{s3}, ω^*_{s4}, and ω^*_{s5}. The dash lines designate unstable equilibria ω^*_{u1}, $\omega^*_{s2,b}$, ω^*_{u2}, ω^*_{u3}, and ω^*_{u4}. The black points denote the saddle-node bifurcation points $P_{sn,a}$, $P_{sn,b}$, $P_{sn,c}$, $P_{sn,d}$, $P_{sn,e}$, $P_{sn,f}$, $P_{sn,g}$, $P_{sn,h}$ and Hopf bifurcation points $P_{H,a}$, $P_{H,b}$.

[17] in particular, because of the restriction on a fixed relationship between the output and the whirling speed of the windmill. The turbine would not revolve at the optimal value till fresh blowing where the wind speed is over the bifurcation point $P_{sn,h}$, i.e., the output power of wind turbine is maximum. A jump phenomenon appears and therefore the stable branch ω^*_{s1} dominates the whirling of the windmill in the place of the branches $\omega^*_{s2,a}$, $\omega^*_{s2,b}$, and $\omega^*_{s2,c}$. However, the phenomenon explain only why the high and low average rotational speeds of the windmill exist together at little wind, but could not explicate the beingness of the disorderly rotational speeds at little wind.

The Hopf bifurcation points $P_{H,a}$ and $P_{H,b}$ on the leading branch ω^*_{s2} could adequatly account for the disorderly rotational speeds of the windmill at low wind speeds. The stable equilibrium points $\omega^*_{s2,a}$ and $\omega^*_{s2,c}$ respectively loss their stability at the Hopf bifurcation points $P_{H,a}$ and $P_{H,b}$ and synchronously generate stable limit cycles which induce the variation of the rotational speeds as the wind speed is larger than 3.91 m/s. In addition, the Hopf bifurcation point $P_{H,b}$ disappears the limit cycles as the wind speed is larger than 7.45 m/s. In the same time, the multiple jump phenomena caused by the saddle-node bifurcation points $P_{sn,d}$, $P_{sn,e}$, $P_{sn,f}$, $P_{sn,g}$ and $P_{sn,h}$ make the rotational speed jumps abruptly. The Hopf and saddle-node bifurcations result in the disorderly rotational speeds of the windmill.

The investigation by Dosaev et al. shows that the nonlinear aerodynamics of the windmill induces some saddle-node bifurcations [18]. Hopf bifurcation would occur in extremly large inductance of a DC genertor which is far away genaral values. However, this study observed that the combination of the nonlinear aerodynamics and electromagnetic field would results in the Hopf and multiple saddle-node bifurcations in a normal inductance of the PMSG. Figure 3 demonstrates that four equilibrium points arise from the intersection of the moment curves of the nonlinear aerodynamics and electromagnetic field. The saddle-node bifurcations result from the fact that pairs of the equilibrium points moving closer and then coalesce each other as varying wind speed. Besides, the dimensionless modelling of the permanent magnet synchronize mechine is similar to the famous Lorenze equation [5]. The Hopf bifurcations are predictably observed in the dynamics of the PMSG.

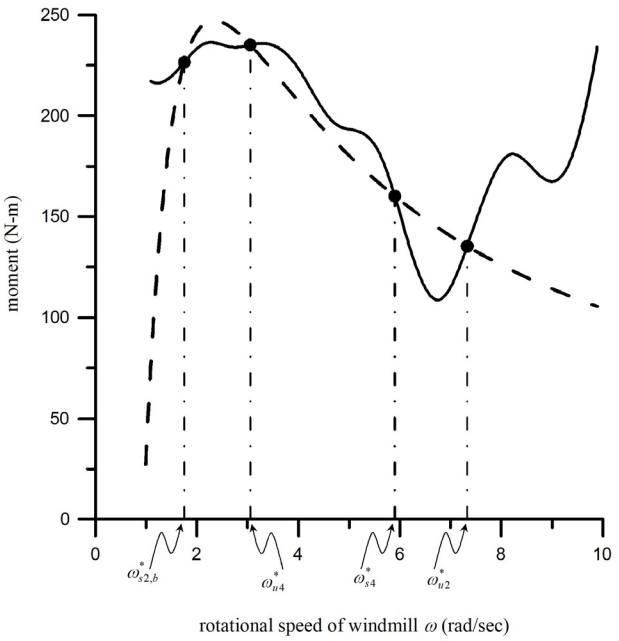

Figure 3. The moment of aerodynamic forces and the induced torque in the PMSG in different staggered rotational speeds of windmill at 7.3 m/s wind speed. The solid line displays the moment of aerodynamic forces. The dash line denotes the induced torque. The symbols $\omega^*_{s2,b}$, ω^*_{s4}, ω^*_{u2}, and ω^*_{u4} are the equilibrium points shown in Figure 2(b).

5 Conclusion

This paper clarified the mechanism of the phenomenon that the variant rotary motion of the windmill appear or vanish once light breeze or fresh blows respectively. Eight saddle-node bifurcations arrange the stable and unstable equilibrium points in a systematic order from the results of analyzing the nonlinear wind rotor. Meanwhile, two Hopf bifurcation points occur due to the nonlinear electromagnetic field of the PMSG. The broad line consisting of the unstable equilibria divide the stable sttractors, including equilibria and limit cycles induced from the Hopf bifurcations, into two sets. The Hopf bifurcations and the broad boundary lead to the disorderly whirling of the small rotor as blowing light to moderate breeze. Moreover, the rightmost saddle-node bifurcation in the right terminal of the line finishes the boundary when strong or fresh breeze blows. The vanishment of the boundary condition eliminates the cluttered rotation and brings the upper side stable equilibrium point, which makes the turbine whirl quickly, to dominate the motion of the windmill. The dynamics would prompt another way of designing the control of small wind turbines optimally through making the saddle-node bifurcation points closer.

References

[1] D. H. Wood, *Small Wind Turbines*, Springer-Verlag, 2011.

[2] A. K. Wright, D. H. Wood, The Starting and Low Wind Speed Behaviour of a Small Horizontal Axis Wind Turbine, *Journal of Wind Engineering and Industrial Aerodynamics*, Vol. 92, No. 14-15, pp. 1265-1279, December, 2004.

[3] L.-S. Shyu, C.-H. Lee, Y.-C. Hsiao, T.-M. Shih, C.-C. Chang, D.-Y. Wang, High-Efficiency 4kW VAWT Design and Development, *Advanced Materials Research*, Vols. 512-515, pp. 617-622, May, 2012.

[4] V. A. Samsonov, M. Z. Dosaev, Y. D. Selyutskiy, Methods of Qualitative Analysis in the Problem of Rigid Body Motion in Medium, *International Journal of Bifurcation and Chaos*, Vol. 21, No. 10, pp. 2955-2961, October, 2011.

[5] Z. Li , J. B. Park, Y. H. Joo, B. Zhang, G, Chen, Bifurcations and Chaos in a Permanent-magnet Synchronous Motor, *IEEE Transactions on Circuits and Systems I: Fundamental Theory and Applications*, Vol. 49, No. 3, pp. 383-387, March, 2002.

[6] H. Ren, D. Liu, Nonlinear Feedback Control of Chaos in Permanent Magnet Synchronous Motor, *IEEE Transactions on Circuits and Systems II: Express Briefs*, Vol. 53, No. 1, pp.45-50, January, 2006.

[7] M. Zribi, A. Oteafy, N. Smaoui, Controlling Chaos in the Permanent Magnet Synchronous Motor, *Chaos, Solitons & Fractals*, Vol. 41, No. 3, pp. 1266-1276, August, 2009.

[8] M. Ataei, A. Kiyoumarsi, B. Ghorbani, Control of Chaos in Permanent Magnet Synchronous Motor by Using Optimal Lyapunov Exponents Placement, *Physics Letters A*, Vol. 374, No. 41, pp. 4226-4230, September, 2010.

[9] H. H. Choi, Adaptive Control of a Chaotic Permanent Magnet Synchronous Motor, *Nonlinear Dynamics*, Vol. 69, No. 3, pp. 1311-1322, August, 2012.

[10] L.-N. Ren, F.-C. Liu, X.-H. Jiao, J,-Y, Li, Hamiltonian Model-based H_∞ Control of Chaos in Permanent Magnet Synchronous Generators for Wind Power Systems, *Acta Physica Sinica*, Vol. 61, No. 6, 060506, March, 2012.

[11] H. Huang, C. Mao, J. Lu, D. Wang, Small-signal Modelling and Analysis of Wind Turbine with Direct Drive Permanent Magnet Synchronous Generator Connected to Power Grid, *IET Renewable Power Generation*, Vol. 6, No. 1, pp. 48-58, January, 2012.

[12] C. Wang, H. Zhang, W. Fan, P. Ma, Analysis of Chaos in High-dimensional Wind Power System, *Chaos*, Vol. 28, No. 1, 013102, January, 2018.

[13] C. Padmanabhan, R. Singh, Analysis of Periodically Excited Non-linear Systems by a Parametric Continuation Technique, *Journal of Sound and Vibration*, Vol. 184, No. 1, pp. 35-58, July, 1995.

[14] S. D. Umans, *Fitzgerald & Kingsley's Electric Machinery*, McGraw-Hill, 2013.

[15] R. E. Sheldahl, P. C. Klimas, *Aerodynamic Characteristics of Seven Symmetrical Airfoil Sections through 180-degree Angle of Attack for Use in Aerodynamic Analysis of Vertical Axis Wind Turbines*, SAND-80-2114, March, 1981.

[16] Y. A. Kuznetsov, *Elements of Applied Bifurcation Theory*, 3rd ed., Springer, 2004.

[17] T. Shiota, T. Isaka, K. Seki, I. Ushiyama, A Passive System for Optimising Battery Charging Using a Permanent Magnet, Variable Speed Generator, *Wind Engineering*, Vol. 35, No. 5, pp. 575-587, October, 2011.

[18] M. Z. Dosaev, V. A. Samsonov, Y. D. Selyutskii, W.-L. Lu, C.-H. Lin, Bifurcation of Operation Modes of Small Wind Power Stations and Optimization of Their Characteristics, *Mechanics of Solids*, Vol. 44, No. 1, pp. 59-66, February, 2009.

Biographies

Yung-Chia Hsiao received the Ph.D. degree in mechanical engineering from National Central University, Taiwan, in 2001. From 2003 to 2019, he was with MingDao University, Taiwan. Now he is with School of Materials Science and Engineering, Baise University, Baise, China. His research interests include dynamics and control of energy systems.

Lih-Shyng Shyu received the Ph.D. degree in mechanical engineering from National Chung-Hsing University, Taiwan, in 2007. From 1989 to 2008, he was with National Chung-Shan Institute of Science and Technology, Taiwan. Since 2008, he is with MingDao University, Taiwan. His research interests include aerodynamics and development of UAVs and wind turbines.